NANO LETTERS

pubs.acs.org/NanoLett

Letter

Solar Seawater Distillation by Flexible and Fully Passive Multistage Membrane Distillation

Wenbin Wang, Yusuf Shi, Chenlin Zhang, Renyuan Li, Mengchun Wu, Sifei Zhuo, Sara Aleid, and Peng Wang*

Cite This: *Nano Lett.* 2021, 21, 5068−5074

Read Online

ACCESS | Metrics & More | Article Recommendations | Supporting Information

ABSTRACT: Solar-assisted distillation is considered promising to solve the freshwater supply for off-grid communities. In this work, a passive and flexible multistage membrane distillation (F-MSMD) device is devised to produce freshwater via solar distillation with the latent heat of vapor condensation being recycled to enhance its energy efficiency. By designing a siphon effect, source water is continuously wicked into the evaporation layer and the concentrated brine flows out of the device before reaching saturation, which successfully solves the otherwise challenge of salt accumulation inside the device. To achieve such siphon flow, the recycled paper is prepared from spent copy paper and used as the evaporation layer for efficient water delivery owing to its large pore size and high hydrophilicity. An eight-stage F-MSMD device exhibits a stable clean water production rate at 3.61 kg m^{-2} h^{-1} in the newly designed siphon-flow mode. This work provides a green route for designing a solar-assisted distillation device.

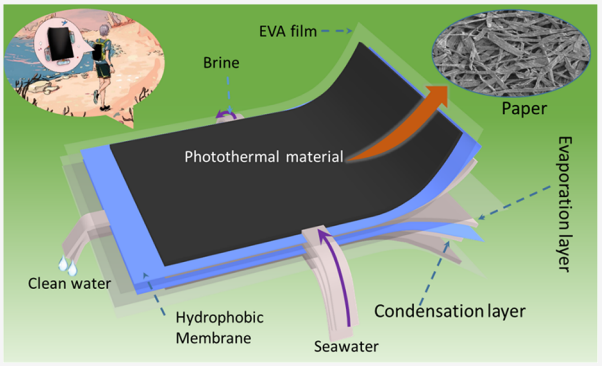

KEYWORDS: *solar distillation, enthalpy recycle, flexible device, paper recycle, off-grid sanitation, portable device, green technology*

INTRODUCTION

Freshwater scarcity is emerging as one of the great challenges in the way of global sustainability.[1−3] As one of 17 sustainable development goals (SDG) established by the United Nations General Assembly in 2015, SDG6 highlights the importance of ensuring availability and sustainable management of water and sanitation for all.[4,5] Although the world has witnessed successful advancement in centralized freshwater supply at urban areas,[6] great challenges remain in freshwater supply in rural and remote regions. Worldwide, over 800 million people do not have daily access to safe drinking water and around 80% of them live in rural regions.[7]

Solar-assisted distillation, which produces freshwater by converting solar energy into heat to drive water evaporation−condensation, is an attractive and suitable option for off-grid freshwater supply in remote regions owing to its low barrier of entry.[8−10] Recent developments in the field are largely focused on the photothermal materials and their structural designs to improve the solar-to-vapor efficiency, with the importance of designing the whole evaporation−condensation system being paid disproportionately less attention. As a matter of fact, the design of the condenser is equally, if not more, significant as it is the "last mile" step to achieve the targeted purpose of freshwater production. A conventional solar-assisted distillation device is composed of a photothermal material or simply bulk water as the evaporator and a transparent cover as the condenser.[11−13] The evaporation−condensation process is driven by the vapor pressure difference between the evaporator and condenser due to their temperature difference. In the conventional solar still, the condenser surface is purposefully designed to be much larger than the area of the evaporator in order to provide large surface area for the dissipation of the large amount of the latent heat released by the vapor condensation. Consequently, the conventional solar-assisted distillation devices are generally rigid, heavy, bulky, and still with an unsatisfactory clean water production rate, typically <1.20 kg m^{-2} h^{-1}.[11,14]

To this end, an energy-efficient, flexible, lightweight, and compact solar-assisted distillation device is highly desired but has not been reported thus far. Such a device, if successfully produced, shall further extend the application breadth of the solar distillation. Recent work has developed a solar-assisted multistage membrane distillation (MSMD) device. In such a device, each stage consists of an evaporation layer, hydrophobic and porous membrane, condensation layer, and thermal conduction layer.[15−18] The latent heat of vapor condensation is recycled to drive another evaporation−condensation process

Received: March 5, 2021
Revised: May 1, 2021
Published: May 27, 2021

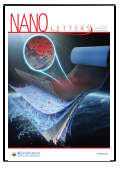

https://doi.org/10.1021/acs.nanolett.1c00910
Nano Lett. 2021, 21, 5068−5074

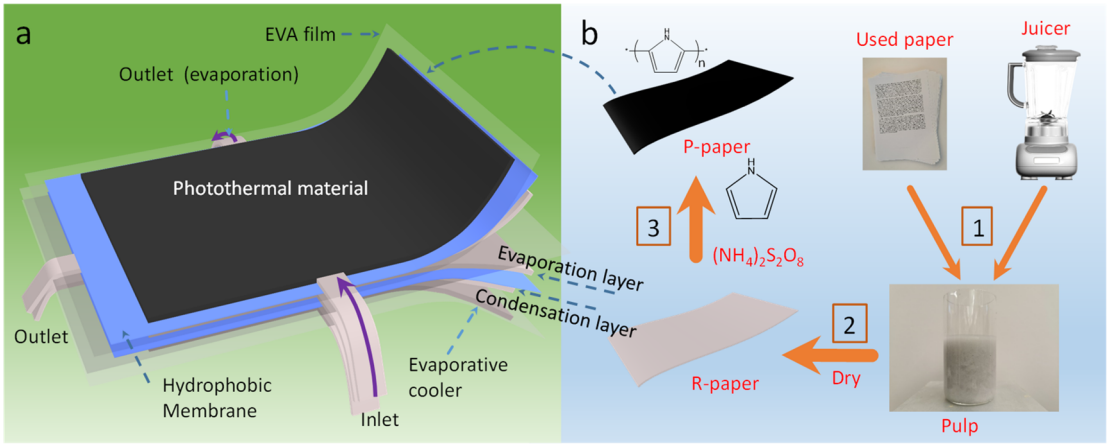

Figure 1. Schematic illustration of the recycle of copy paper and structure of the flexible multistage membrane distillation device: (a) schematics of two-stage flexible paper-based MSMD; (b) recycle procedure of the copy paper (steps 1 and 2) and modification of the recycled paper by polypyrrole (step 3).

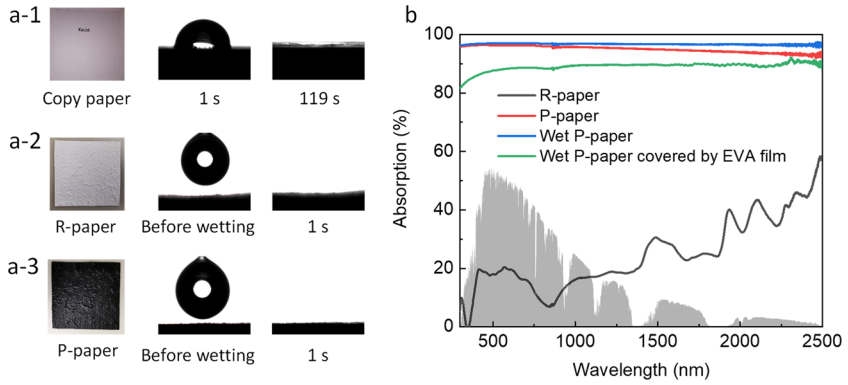

Figure 2. Wettability of the paper and their UV−vis−NIR spectrum: (a-1 to a-3) contact angles of water on raw copy paper, recycled paper (R-paper), and polypyrrole modified R-paper (P-paper); (b) UV−vis−NIR spectrum of the papers.

rather than dissipating into the ambient environment. Due to the recycle of the latent heat, no extra heat dissipation surface is demanded and the area of the condenser can be designed to be equivalent to that of the evaporator. However, the challenge remains in how to design a flexible MSMD device with a high desalination performance, which requires a holistic optimization of materials preparation and selection, light absorption, heat management, water transportation, among others.

Herein, we demonstrate a fully passive and flexible multistage membrane distillation (F-MSMD) device with the state-of-the-art solar real seawater desalination performance. The design of the F-MSMD device is based on a compact direct contact membrane distillation design within each stage. The thickness of a typical eight-stage F-MSMD is less than 2 cm, while it compares very favorably against the thickness of >10 cm of the traditional solar distillation devices.[11,12,19] The evaporation layer in F-MSMD is made of the recycled copy paper (R-paper). A fully passive siphon-flow mode is devised in F-MSMD to allow the concentrated brine produced to flow out before reaching saturation and thus solves the salt accumulation issue in the evaporation layer.

As a proof-of-concept, an eight-stage F-MSMD device was fabricated, and it exhibited a clean water production rate of 3.61 kg m^{-2} h^{-1} for real seawater desalination, which is comparable to the state-of-the-art solar-assisted seawater distillation performances reported in the literature. It needs to be pointed out that real seawater was employed to evaluate the seawater desalination performance in this work as compared to many literature works using 3.5% NaCl as seawater surrogate.[20−23] The F-MSMD device subversively changes the rigid physical form of the conventional solar distillation system and opens the possibility of MSMD being applied in such mobile situations as camping and hiking. The results of this work shine lights on further developing solar distillation processes toward practical applications in real scenarios and will inspire more research efforts to be diverted into this important topic.

RESULTS AND DISCUSSION

Structure of the Multistage Membrane Distillation Device. The structure of the F-MSMD device is shown in Figure 1a and Figure S1. Each stage consists of a transparent thermal conduction layer, evaporation layer, hydrophobic porous membrane, and condensation layer. Additionally, an evaporative cooler is designed under the device to dissipate the low-grade latent heat of the last stage by evaporating the source water. During operation, the water is delivered by siphon effect, which demands the materials in the evaporation layer to be hydrophilic and have a large pore size to enhance the flow rate. To this end, we developed a simple method to prepare a recycled paper (R-paper) from commercial copy paper (Figure 2b), which was used as evaporation layer and condensation layer. Moreover, the PPy coated paper (P-paper), which is obtained by modifying the R-paper with PPy, is used as the

https://doi.org/10.1021/acs.nanolett.1c00910
Nano Lett. 2021, 21, 5068−5074

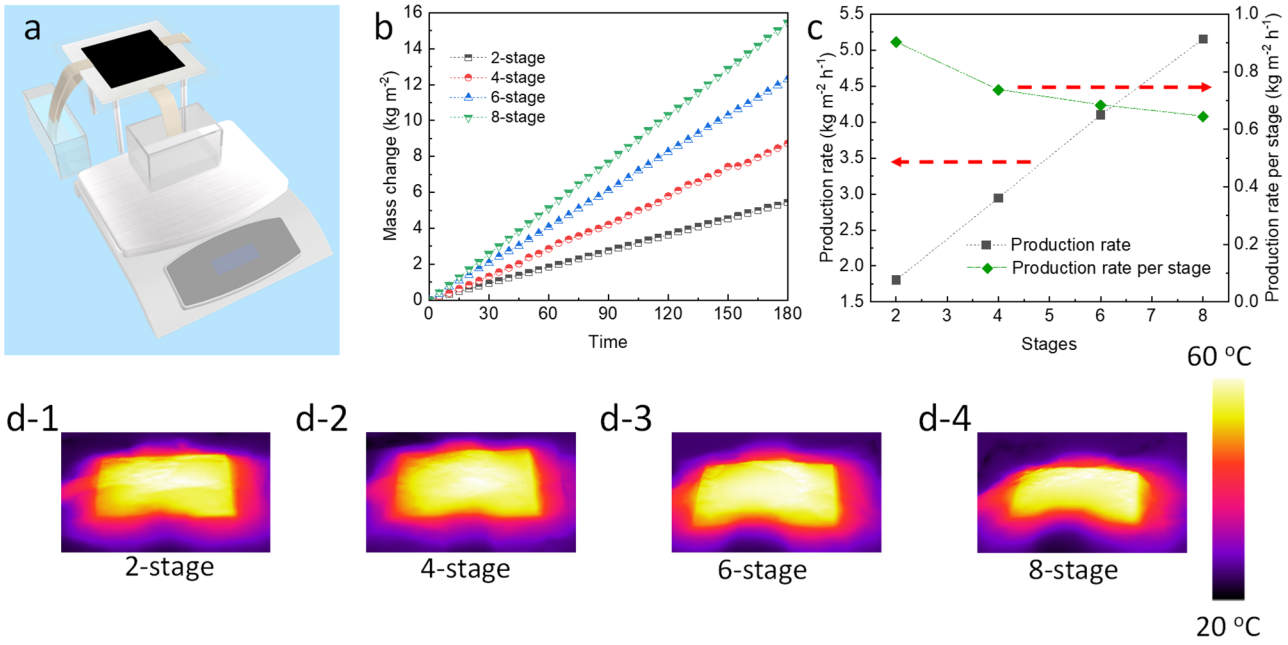

Figure 3. Clean water production performance of the F-MSMD device: (a) experimental setup; (b) mass change of the collected clean water from F-MSMD at different stages under one sun illumination; (c) relation between the clean water production rate and number of stages; (d-1 to d-4) IR image of the photothermal layer in F-MSMD device with different number of stages.

photothermal material in the top evaporation layer for sunlight absorption (see more details in Figures S2 and S3, Supporting Information).

Hydrophilicity of the Paper. The hydrophilicity of the paper was evaluated by its contact angle of water. As shown in Figure 2a-1, the raw copy paper exhibited an initial hydrophobicity with a contact angle of 105°, and after around 118 s, the water was completely adsorbed by the paper, indicating that the paper turned hydrophilic after sufficient contact with water. In comparison, 1 s after the water was dropped on the R-paper (Figure 2a-2), it was completely adsorbed, demonstrating that the R-paper was hydrophilic. The wettability change is presumably attributed to the removal of the hydrophobic pigments from the raw commercial copy paper in the process of the water removal from the formed pulp via filtration. Additionally, after the R-paper was modified by PPy, the obtained P-paper exhibited comparable hydrophilicity with respect to R-paper (Figure 2a-3), indicating that the PPy modification has little effect on the hydrophilicity of the R-paper. The SEM images of the raw copy paper, R-paper, and P-paper are shown in Figure S4. As seen, the raw copy paper is assembled by fibers in compact structure while in the R-paper and P-paper, the fibers are assembled more loosely. The pore sizes of P-paper and R-paper are over 20 μm, while the pore size of the raw copy paper is mostly below 5 μm. It is known that elevating the pore size in porous materials increases the capillary-induced flow rate.[24−26] Therefore, the water flow rate in R-paper and P-paper is expected to be higher relative to the raw copy paper.

Solar Absorptance of the P-Paper. The UV−vis−NIR absorption spectra of the obtained R-paper and P-paper were collected and shown in Figure 2b. The P-paper exhibited a high light absorption between the wavelengths of 300 and 2500 nm, while the R-paper delivered a weak light absorption. The solar absorptance values of the R-paper and P-paper (calculated from a weight fraction between absorbed radiation energy and incoming solar radiation energy)[14] are 0.96 and 0.17, respectively. Since the absorption of the porous material can be affected by its working state (dry or wet) due to the different refractive index of the air, water, cellulose, and PPy, the absorption of the wet P-paper was also measured and the solar absorptance was calculated to be 0.97. Moreover, in the F-MSMD device, the P-paper was covered by a piece of transparent EVA film and part of the sunlight was reflected or absorbed by the EVA film. Note that as long as the sunlight is not reflected, the sunlight absorbed by the EVA film is also largely used by the F-MSMD system. Therefore, the solar absorptance of the F-MSMD system was equivalent to the solar absorptance of the wet P-paper covered by EVA film, and the corresponding solar absorptance was measured to be at 0.89.

Clean Water Production Performance. The clean water production performance of the F-MSMD device was first evaluated by a homemade experimental setup (Figure 3a) under one-sun radiation with pure water as source water in the dead-end mode. The mass change of the collected clean water was monitored and presented in Figure 3b. The average clean water production rates of two-stage, four-stage, six-stage, and eight-stage F-MSMD device (calculated from the slope of the mass change curve) were 1.81, 2.95, 4.10, and 5.15 kg m^{-2} h^{-1}, respectively. A linear relation between the clean water production rate and the number of stages of the F-MSMD can be found (Figure 3c). Besides, the clean water production rates per stage of the two-stage, four-stage, six-stage, and eight-stage F-MSMD devices were calculated to be 0.91, 0.74, 0.68, and 0.64 kg m^{-2} h^{-1}, respectively, indicating that further addition of stages decreases the clean water production rate per stage. The temperature of the top photothermal evaporation layers in the four devices was monitored by infrared camera (IR). As presented in Figure 3d-1 to d-4, all of them show an uneven temperature distribution, varying within the range of 40−60 °C, which should be resulting from the low thermal conductivity of the wet P-paper. The porosity of R-paper and P-paper was around 0.90 and 0.88, respectively, and the

https://doi.org/10.1021/acs.nanolett.1c00910
Nano Lett. 2021, 21, 5068−5074

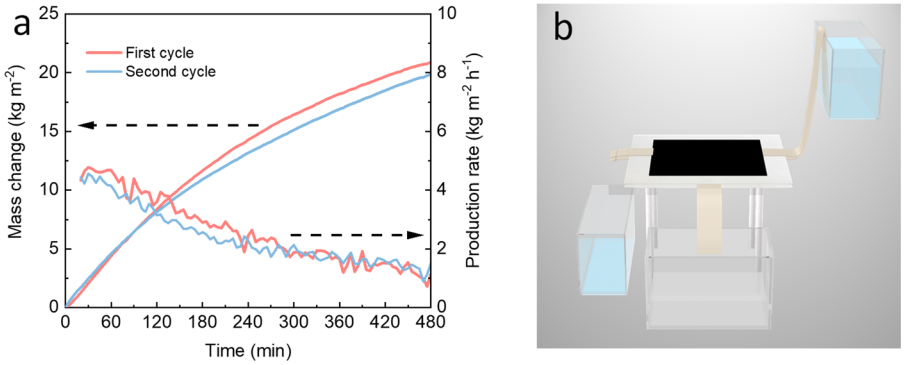

Figure 4. Seawater desalination performance of the F-MSMD device working in the dead-end mode: (a) mass change of the collected clean water from F-MSDM device using seawater as source water and the corresponding clean water production rate; (b) rinsing process of the F-MSMD device by raw seawater.

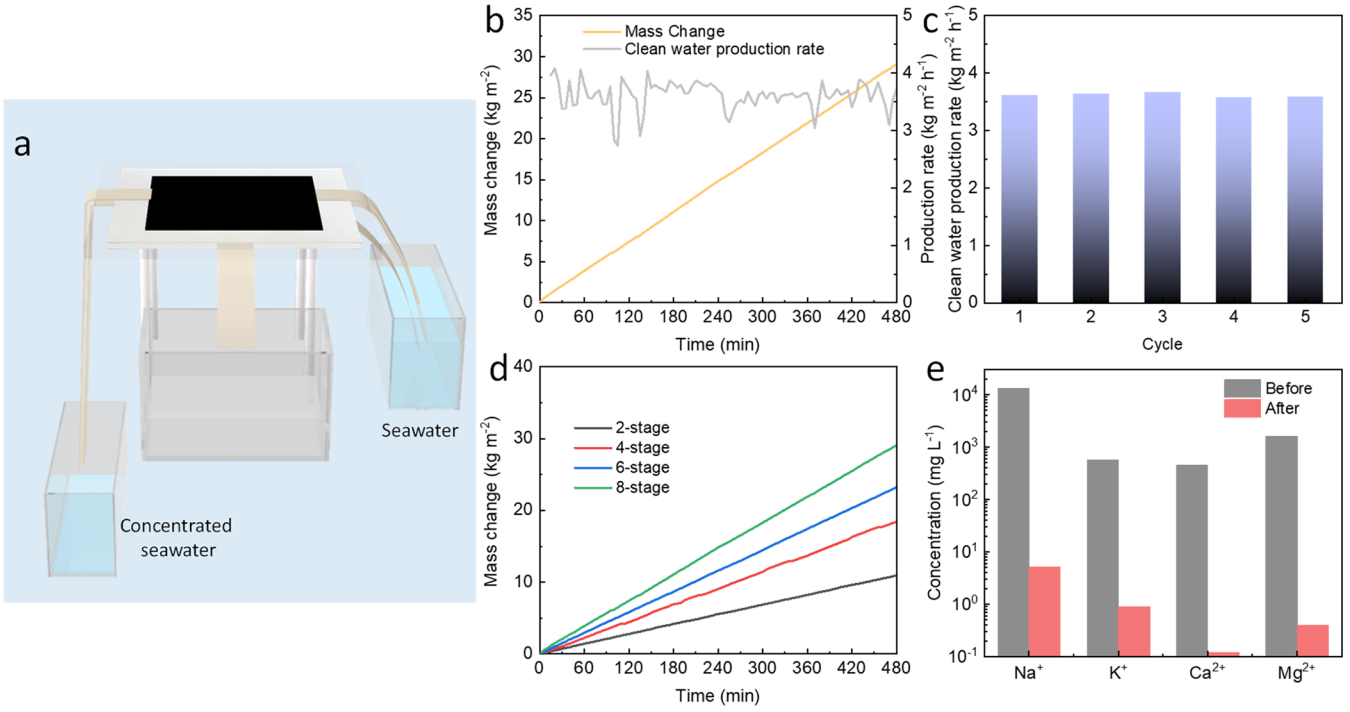

Figure 5. Seawater desalination performance of the F-MSMD device working in siphon-flow mode: (a) experimental setup of the F-MSMD device working in siphon-flow mode; (b) mass change of the collected clean water and the corresponding clean water production rate when seawater was used as source water under one-sun illumination; (c) clean water production rate in five cycles; (d) mass change of the collected water from F-MSMD with different stages; (e) ion concentration in the collected water and raw seawater.

thermal conductivity of wet paper is assumed to be lower than that of water (0.6 W m^{-1} K^{-1}) considering that the space of the wet paper is occupied by water and small air bubbles. The area, where the temperature was higher than 50 °C, was marked in Figure S5, which presents an increasing proportion with the increment in the number of stages, indicating that the photothermal evaporation layer in the devices with more stages had a higher temperature. As a result, more heat was lost by thermal radiation, leading to a lower clean water production rate per stage as the number of stages increased.

Seawater Desalination in Dead-End Mode. The F-MSMD device is aiming to be applied to desalinate various quality-impaired source water, such as brine, seawater, and brackish water. In this work, we adopted the real Red Sea seawater to evaluate its clean water production performance. Compared to 3.5% NaCl solution that is typically utilized as seawater surrogate in considerable amount of literatures,[20−22,27] desalinating real seawater is more challenging because the crystallization of the minor species, e.g., $MgSO_4$, can cause the clogging of the porous structure, resulting in a massive reduction in evaporation rate.[28] It was recently reported that this problem can be solved by adding trace amount of nitrilotriacetic acid (NTA) into the real seawater (more details can be found in Figure S6 and Supporting Information). To this end, the real seawater was pretreated by adding small amounts of NTA (10 ppm). As shown in Figure 4a, the eight-stage F-MSMD device working in the dead-end mode exhibited a monotonically reduced clean water production rate from 4.34 kg m^{-2} h^{-1} to 1.39 kg m^{-2} h^{-1} during the 8 h illumination. The average clean water production rate was calculated to be 2.62 kg m^{-2} h^{-1}. As compared to the case with pure water as source water at 5.15 kg m^{-2} h^{-1}, the device showed a lower initial clean water

https://doi.org/10.1021/acs.nanolett.1c00910
Nano Lett. 2021, 21, 5068−5074

production rate, which should be attributed to the lower saturated vapor pressure of the seawater.

To remove the salt inside the pores in the evaporation layer, the evaporation layer was rinsed by the raw seawater. As shown in Figure 4b, the source water container was lifted to be higher than the device, allowing the seawater to flow across and through the evaporation layer before finally exiting from the outlet on the other side. The salt inside the pores can be redissolved and taken away by the flowing seawater−water. After rinsing the evaporation layers overnight, the source water container was placed back to its original position and the seawater desalination test was conducted again (second cycle). As shown in Figure 4a (red line), the device exhibited only slightly compromised clean water production rate of around 2.50 kg m^{-2} h^{-1}, indicating that the seawater desalination performance can be largely recovered by the rinsing procedure.

The temperature of a fixed point in the top photothermal layer (Figure S7) was continuously monitored in the course of the experiments. Although such a point does not represent the temperature of the whole photothermal layer, the point and the whole photothermal layer have a synchronous temperature change. As shown in Figure S7, the temperature of this point increased greatly from the ambient temperature to 53.1 °C in 8 h. The highest temperature of the top evaporation layer at the end of the experiment was measured to be 69.4 °C, which is much higher than the scenario with pure water as source water. The temperature rise should be attributed to the gradual pore clogging of the evaporation layer because when the pores are occupied by the crystallized salts, the seawater transport and evaporation would be inhibited. Consequently, a higher temperature is the result, leading to more thermal radiation energy loss and thus reduced clean water production rate.

Seawater Desalination at Siphon-Flow Mode. To address the challenge of the pore clogging and desalination performance reduction in the dead-end mode, the siphon-flow mode was then designed (Figure 5a). The source water was first wicked into the evaporation layer and then dripped down from the end of the strip on the outlet side. The flow rate of the seawater across the evaporation layer driven by this siphon-flow mode was investigated under both dark and illumination conditions. Herein, we use the term "discharge rate" to represent water flow rate as it was evaluated by measuring the mass change of the collected source water from the outlet. As shown in Figure S8, the system exhibited a stable discharge rate in the dark of 2.93 kg m^{-2} h^{-1}. Once the light was switched on, the discharge rate decreased dramatically to <1.5 kg m^{-2} h^{-1}, and in the next 8 h, the discharge rate showed a descending trend owing to the decline in the water level in the source water container. The average discharge rate under illumination was around 0.88 kg m^{-2} h^{-1}. Under illumination, when the liquid water passes through the evaporation layer, part of liquid water is evaporated and condensed in the condensation layer. As a result, less water flows to the outlet, leading to a reduced discharge rate. After the light was turned off, the water discharge rate was increased back to 2.72 kg m^{-2} h^{-1}, which is slightly lower than that before illumination. The reduced flow rate should be attributed to the water level drop in the source water container (around ∼0.5 cm). The mass change of the collected clean water was monitored simultaneously, and the results are presented in Figure 5b. At the siphon-flow mode, the device exhibited a stable clean water production rate during the 8 h illumination at around 3.61 kg m^{-2} h^{-1}, which is much higher than the average clean water production rate when the device worked in the dead-end mode (i.e., 2.62 kg m^{-2} h^{-1}). It is worth emphasizing that the water discharge rate in the dark is not equivalent to the sum of water evaporation rate and water discharge rate under illumination, because the evaporation of water from the pores creates a negative pressure, providing an extra driving force to pull the water out of the source water container. Such passive water transport is similar to the transpiration of the plant. These results demonstrate that the newly designed siphon-flow mode is capable of eliminating the salt accumulation in the evaporation layer during seawater distillation, allowing the device to have a stable clean water production rate. As shown in Figure S9, the temperature of a certain point in the top photothermal layer exhibited stable change with a slightly increased trend from ambient temperature to 37.1 °C in 8 h. The top evaporation layer showed a maximum temperature of 58.2 °C at the end of the experiment, which is much lower relative to the case that the device works in the dead-end mode.

After illumination, the device was kept in the dark overnight, allowing the source water to continuously rinse the evaporation layer. The following four cycles were conducted under the otherwise the same conditions. As shown in Figure 5c, the clean water production rate of the F-MSMD device working at siphon-flow mode in the five cycles changed slightly within the range of 3.57−3.66 kg m^{-2} h^{-1}, exhibiting an excellent operation durability. Moreover, when seawater was used as source water, one may raise the concern that small amounts of additives and stains remaining in the R-paper can affect the performance of the device. To this end, the pulp was washed 10 times to ensure the removal of the additives and the prepared R-paper was used to fabricate a new eight-stage F-MSMD device. As shown in Figure S10, the device exhibited a comparable clean water production rate of 3.62 kg m^{-2} h^{-1}, confirming that the small amounts of additives remaining in the paper have little effect on the performance of the device. The seawater desalination performance of the F-MSMD device at different number of stages was also measured (Figure 5d), and the clean water production rates were 1.37 kg m^{-2} h^{-1} for two-stage, 2.32 kg m^{-2} h^{-1} for four-stage, and 2.90 kg m^{-2} h^{-1} for six-stage. The ion concentrations of the collected water and source water were measured by ICP-OES, and the results are shown in Figure 5e. The results demonstrate that the major ion (i.e., Na^+, K^+, Ca^{2+}, Mg^{2+}) concentrations of the collected water were all lower than 10 ppm, indicating satisfactory water quality for meeting the drinking water guideline of World Health Organization (WHO) for these ions. Moreover, no carbon species was detected in the collected clean water by total organic carbon (TOC), indicating that the NTA was not evaporated during distillation. This result further demonstrates that collected clean water is safe enough for drinking.

A larger eight-stage F-MSMD device (10 cm × 10 cm) was further fabricated for the outdoor test. As presented in Figure S11a,b, the F-MSMD device is easily rolled up, manifesting its good flexibility. The outdoor experiment was conducted on the campus of King Abdullah University of Science and Technology (Thuwal, Saudi Arabia). The experimental setup is shown in Figure S12 and Figure S13a, while the ambient environmental conditions during the experiment are presented in Figure S13b. With a total solar power of 5.06 kWh m^{-2}, the eight-stage F-MSMD large device exhibited a clean water production rate of 16 kg m^{-2} per day, which is enough to meet

https://doi.org/10.1021/acs.nanolett.1c00910
Nano Lett. 2021, 21, 5068−5074

the minimal drinking water demands for at least four adults per day.

CONCLUSION

We developed a flexible multistage membrane distillation device (F-MSMD). Highly efficient solar water desalination was achieved by utilizing recycled paper as the primary material in the F-MSMD device. In seawater desalination, a stable clean water production rate of 3.61 kg m^{-2} h^{-1} was realized by developing a newly designed siphon-flow operation mode, which avoids the salt accumulation in the device. Developing such a flexible device can make the solar water distillation device become portable, flexible, and lightweight so that its application can be further extended to some other situations such as hiking and camping.

ASSOCIATED CONTENT

Supporting Information

The Supporting Information is available free of charge at https://pubs.acs.org/doi/10.1021/acs.nanolett.1c00910.

Additional notes and figures, including experimental section, structure of the F-MSMD device, siphon-flow mode, SEM images of the paper, IR images, picture of salt crystallization, flow rate of source water in siphon-flow mode, picture of the flexible F-MSMD device in folded and unfolded state, and results of outdoor test (PDF)

AUTHOR INFORMATION

Corresponding Author

Peng Wang − *Water Desalination and Reuse Center, Division of Biological and Environmental Science and Engineering, King Abdullah University of Science and Technology, Thuwal 23955-6900, Saudi Arabia; Department of Civil and Environmental Engineering, Hong Kong Polytechnic University, Hong Kong, China;* orcid.org/0000-0003-0856-0865; Email: peng.wang@kaust.edu.sa

Authors

Wenbin Wang − *Water Desalination and Reuse Center, Division of Biological and Environmental Science and Engineering, King Abdullah University of Science and Technology, Thuwal 23955-6900, Saudi Arabia;* orcid.org/0000-0002-0541-6609

Yusuf Shi − *Water Desalination and Reuse Center, Division of Biological and Environmental Science and Engineering, King Abdullah University of Science and Technology, Thuwal 23955-6900, Saudi Arabia;* orcid.org/0000-0003-1304-5737

Chenlin Zhang − *Water Desalination and Reuse Center, Division of Biological and Environmental Science and Engineering, King Abdullah University of Science and Technology, Thuwal 23955-6900, Saudi Arabia*

Renyuan Li − *Water Desalination and Reuse Center, Division of Biological and Environmental Science and Engineering, King Abdullah University of Science and Technology, Thuwal 23955-6900, Saudi Arabia;* orcid.org/0000-0003-1943-9403

Mengchun Wu − *Water Desalination and Reuse Center, Division of Biological and Environmental Science and Engineering, King Abdullah University of Science and Technology, Thuwal 23955-6900, Saudi Arabia;* orcid.org/0000-0003-4647-110X

Sifei Zhuo − *Water Desalination and Reuse Center, Division of Biological and Environmental Science and Engineering, King Abdullah University of Science and Technology, Thuwal 23955-6900, Saudi Arabia*

Sara Aleid − *Water Desalination and Reuse Center, Division of Biological and Environmental Science and Engineering, King Abdullah University of Science and Technology, Thuwal 23955-6900, Saudi Arabia*

Complete contact information is available at: https://pubs.acs.org/10.1021/acs.nanolett.1c00910

Author Contributions

W.W., Y.S., and P.W. conceived the idea. W.W. and P.W. designed the experiments. W.W. conducted the experiments. C.Z. and R.L. helped in the SEM measurement. M.W. and R.L. helped draw the schematics. Y.S., W.W., M.W., C.Z., S.Z., S.A., and P.W. all contributed to writing and revising the paper.

Notes

The authors declare no competing financial interest.

REFERENCES

(1) Chen, C. J.; Kuang, Y. D.; Hu, L. B. Challenges and opportunities for solar evaporation. *Joule* **2019**, *3* (3), 683−718.

(2) Guo, Y.; Bae, J.; Fang, Z.; Li, P.; Zhao, F.; Yu, G. Hydrogels and hydrogel-derived materials for energy and water sustainability. *Chem. Rev.* **2020**, *120* (15), 7642−7707.

(3) Finnerty, C.; Zhang, L.; Sedlak, D. L.; Nelson, K. L.; Mi, B. Synthetic graphene oxide leaf for solar desalination with zero liquid discharge. *Environ. Sci. Technol.* **2017**, *51* (20), 11701−11709.

(4) Ortigara, A. R. C.; Kay, M.; Uhlenbrook, S. A review of the sdg 6 synthesis report 2018 from an education, training, and research perspective. *Water* **2018**, *10* (10), 1353.

(5) McCollum, D.; Gomez Echeverri, L.; Riahi, K.; Parkinson, S. SDG7: Ensure access to affordable, reliable, sustainable and modern energy for all. In *A Guide to SDG Interactions: From Science to Implementation*; ICSU, 2017; pp 127−173.

(6) Qasim, M.; Badrelzaman, M.; Darwish, N. N.; Darwish, N. A.; Hilal, N. Reverse osmosis desalination: A state-of-the-art review. *Desalination* **2019**, *459*, 59−104.

(7) Gomez, M.; Perdiguero, J.; Sanz, A. Socioeconomic factors affecting water access in rural areas of low and middle income countries. *Water* **2019**, *11* (2), 202.

(8) Xu, Y.; Tang, C.; Ma, J.; Liu, D.; Qi, D.; You, S.; Cui, F.; Wei, Y.; Wang, W. Low-tortuosity water microchannels boosting energy utilization for high water flux solar distillation. *Environ. Sci. Technol.* **2020**, *54* (8), 5150−5158.

(9) Yuan, Y.; Dong, C.; Gu, J.; Liu, Q.; Xu, J.; Zhou, C.; Song, G.; Chen, W.; Yao, L.; Zhang, D. A scalable nickel-cellulose hybrid metamaterial with broadband light absorption for efficient solar distillation. *Adv. Mater.* **2020**, *32* (17), 1907975.

(10) Li, X. Q.; Min, X. Z.; Li, J. L.; Xu, N.; Zhu, P. C.; Zhu, B.; Zhu, S. N.; Zhu, J. Storage and recycling of interfacial solar steam enthalpy. *Joule* **2018**, *2* (11), 2477−2484.

(11) Zhang, L.; Tang, B.; Wu, J.; Li, R.; Wang, P. Hydrophobic light-to-heat conversion membranes with self-healing ability for interfacial solar heating. *Adv. Mater.* **2015**, *27* (33), 4889−94.

(12) Ni, G.; Zandavi, S. H.; Javid, S. M.; Boriskina, S. V.; Cooper, T. A.; Chen, G. A salt-rejecting floating solar still for low-cost desalination. *Energy Environ. Sci.* **2018**, *11* (6), 1510−1519.

(13) Yang, Y.; Zhao, R.; Zhang, T.; Zhao, K.; Xiao, P.; Ma, Y.; Ajayan, P. M.; Shi, G.; Chen, Y. Graphene-based standalone solar energy converter for water desalination and purification. *ACS Nano* **2018**, *12* (1), 829−835.

(14) Shi, Y.; Li, R. Y.; Jin, Y.; Zhuo, S. F.; Shi, L.; Chang, J.; Hong, S.; Ng, K. C.; Wang, P. A 3d photothermal structure toward improved energy efficiency in solar steam generation. *Joule* **2018**, *2* (6), 1171−1186.
(15) Xue, G.; Chen, Q.; Lin, S.; Duan, J.; Yang, P.; Liu, K.; Li, J.; Zhou, J. Highly efficient water harvesting with optimized solar thermal membrane distillation device. *Glob Chall* **2018**, *2* (5−6), 1800001.
(16) Chiavazzo, E.; Morciano, M.; Viglino, F.; Fasano, M.; Asinari, P. Passive solar high-yield seawater desalination by modular and low-cost distillation. *Nature Sustainability* **2018**, *1* (12), 763−772.
(17) Xu, Z. Y.; Zhang, L. N.; Zhao, L.; Li, B. J.; Bhatia, B.; Wang, C. X.; Wilke, K. L.; Song, Y.; Labban, O.; Lienhard, J. H.; Wang, R. Z.; Wang, E. N. Ultrahigh-efficiency desalination via a thermally-localized multistage solar still. *Energy Environ. Sci.* **2020**, *13* (3), 830−839.
(18) Zhang, L. N.; Xu, Z. Y.; Bhatia, B.; Li, B. J.; Zhao, L.; Wang, E. N. Modeling and performance analysis of high-efficiency thermally-localized multistage solar stills. *Appl. Energy* **2020**, *266*, 114864.
(19) Deshmukh, H. S.; Thombre, S. B. Solar distillation with single basin solar still using sensible heat storage materials. *Desalination* **2017**, *410*, 91−98.
(20) Shi, Y.; Zhang, C.; Li, R.; Zhuo, S.; Jin, Y.; Shi, L.; Hong, S.; Chang, J.; Ong, C.; Wang, P. Solar evaporator with controlled salt precipitation for zero liquid discharge desalination. *Environ. Sci. Technol.* **2018**, *52* (20), 11822−11830.
(21) Zhang, Q.; Yang, H. J.; Xiao, X. F.; Wang, H.; Yan, L.; Shi, Z. X.; Chen, Y. L.; Xu, W. L.; Wang, X. B. A new self-desalting solar evaporation system based on a vertically oriented porous polyacrylonitrile foam. *J. Mater. Chem. A* **2019**, *7* (24), 14620−14628.
(22) Wang, X.; Gan, M.; Chen, R.; Peng, H.; Zhang, T. Q.; Ye, M. M. Water delivery channel design in solar evaporator for efficient and durable water evaporation with salt rejection. *ACS Sustainable Chem. Eng.* **2020**, *8* (21), 7753−7761.
(23) Khan, M. A. S.; Singh, A.; Haldar, S.; Ganguly, B. Can nitrilotriacetic acid (nta) act as a habit modifier for rock salt crystals? An answer from computational and experimental studies. *Cryst. Growth Des.* **2011**, *11* (5), 1675−1682.
(24) Ansari, N.; Kish, M. H. The wicking of water in yarn as measured by an electrical resistance technique. *J. Text. Inst.* **2000**, *91* (3), 410−419.
(25) Hollies, N. R.; Kaessinger, M. M.; Bogaty, H. Water transport mechanisms in textile materials1 part i: The role of yarn roughness in capillary-type penetration. *Text. Res. J.* **1956**, *26* (11), 829−835.
(26) Li, T.; Liu, H.; Zhao, X. P.; Chen, G.; Dai, J. Q.; Pastel, G.; Jia, C.; Chen, C. J.; Hitz, E.; Siddhartha, D.; Yang, R. G.; Hu, L. B. Scalable and highly efficient mesoporous wood-based solar steam generation device: Localized heat, rapid water transport. *Adv. Funct. Mater.* **2018**, *28* (16), 1707134.
(27) Zhou, X.; Guo, Y.; Zhao, F.; Shi, W.; Yu, G. Topology-controlled hydration of polymer network in hydrogels for solar-driven wastewater treatment. *Adv. Mater.* **2020**, *32* (52), 2007012.
(28) Zhang, C.; Shi, Y.; Shi, L.; Li, H.; Li, R.; Hong, S.; Zhuo, S.; Zhang, T.; Wang, P. Designing a next generation solar crystallizer for real seawater brine treatment with zero liquid discharge. *Nat. Commun.* **2021**, *12* (1), 998.

https://doi.org/10.1021/acs.nanolett.1c00910
Nano Lett. 2021, 21, 5068−5074